Doppler-Free Two-Photon Spectroscopy of Hydrogen Rydberg States: Remeasurement of R_∞

M. Allegrini, F. Biraben, B. Cagnac, J.C. Garreau, and L. Julien*

Laboratoire de Spectroscopie Hertzienne de l'ENS**,
4, Place Jussieu, Tour 12 1er étage,
F-75252 Paris Cedex 05, France
* Permanent Address: Istituto di Fisica Atomica e Molecolare del CNR, Pisa, Italy
**Laboratoire associé au CNRS: UA18

1. Introduction

In the last few years, the application of very high resolution laser spectroscopy to atomic hydrogen has allowed the determination of the Rydberg constant with an increasing precision up to a few parts in 10^{10} /1-7/. Because R_∞ plays a key role in atomic physics, quantum electrodynamics and metrology, it is desirable to improve even further this precision ; experiments to this aim are currently being performed in various laboratories. In this work we report on latest measurements of R_∞ which are in fact limited by the precision of the wavelength standard in the optical domain (1.6×10^{-10}).

The method we use is Doppler free two-photon laser spectroscopy, applied to the atomic hydrogen transitions from the metastable 2S state to the Rydberg nD states (n = 8, 10, 12) /8/.

Compared to the method based on the study of the 2S-3P /4/ or 2S-4P /5/ one-photon transitions, our method takes advantage of the narrow linewidths of the Rydberg levels ($\sim$ 300kHz for the 10D level). From this point of view, the 1S-2S two-photon transition with a natural linewidth of 1.3 Hz offers in principle the best experimental resolution. However, this transition is affected by the uncertainty on the 1S Lamb shift, while the 2S Lamb shift has been measured with a very high precision and the nD Rydberg levels have negligible Lamb shifts. Thus the measurement of the 1S-2S frequency /6,7/ provides an experimental value of the 1S Lamb shift rather than an independent value of the Rydberg constant.

The Hydrogen Atom Editors: G.F. Bassani · M. Inguscio · T.W. Hänsch

2. Experimental method and apparatus

The apparatus consists of two major parts : (i) the vacuum chamber where the beam of metastable 2S atoms is produced, excited to the nD levels and detected (Fig.1) ;(ii) the optical system with the lasers used for the excitation and for the control of the transition frequency (Fig.2).

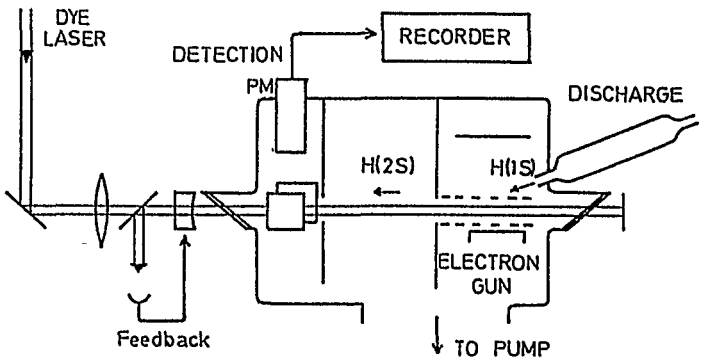

Figure 1 : Metastable beam apparatus

The metastable atomic beam is produced in two steps : molecular hydrogen flowing in a pyrex tube is dissociated by a radiofrequency discharge and the resulting ground state effusive beam enters in a first vacuum chamber ; then atoms are excited to the 2S state by electronic bombardment. Because of the inelastic collisions with electrons, the atomic beam is deviated by about 20°. The optical absorption takes place in a second vacuum chamber evacuated by two cryogenic pumps and where electric and magnetic fields are reduced as much as possible. In this chamber the metastable atomic beam is collinear with two counterpropagating laser beams, in order to reduce the line broadening due to the finite transit time of the atoms in the laser beams. Metastable atoms are detected in a third chamber where an electric field is applied to mix the 2S with the 2P levels and the resulting Lyman α radiation is measured.

The light source is a home made CW ring LD 700 dye laser, pumped by a Kr^+ laser. In the range 730-780 nm (wavelength of the two-photon 2S-nD transitions for $n \geq 8$) it provides a power of about 1W on single mode operation. The frequency stabilization is made by locking the laser to an external auxiliary Fabry-Perot cavity indicated FPA in Fig.2 ; the resulting linewidth is about 50 kHz.

A Fabry-Perot cavity (shown in Fig.1) having its optical axis coincident with the metastable atomic beam provides a standing wave that induces the two-photon transitions. This cavity is locked to the laser frequency in order to increase the intensity of the standing wave to ~ 50W in each propagation direction.

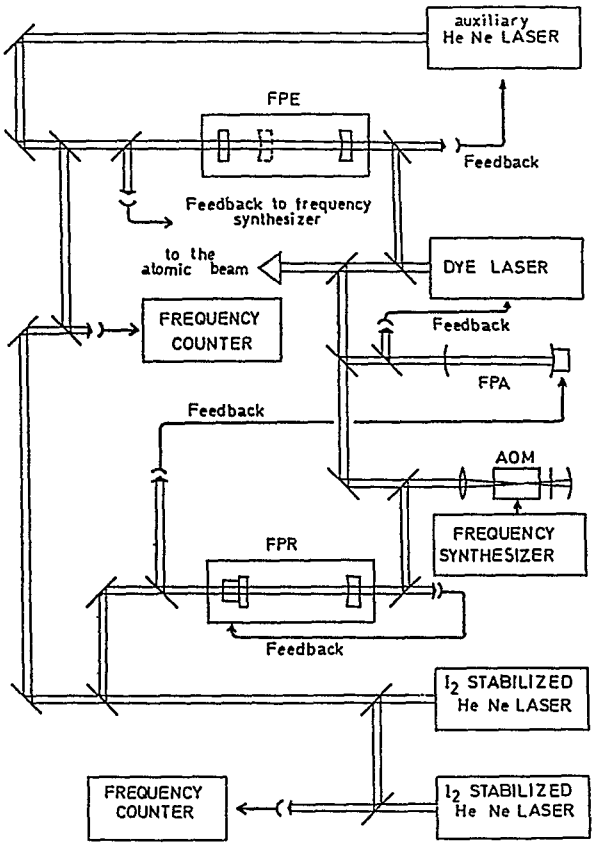

Figure 2 : Experimental set-up for the control and the measurement of the dye laser frequency

To sweep the dye laser its beam is split and the secondary beam is driven into an acousto-optic device. The frequency-shifted beam is reflected back into the acousto-optic crystal so that one of the emerging beams is shifted twice. This beam then enters a reference Fabry-Perot cavity (indicated as FPR in Fig. 2) of very high finesse, whose length is locked to an I_2 - stabilized

He-Ne laser. The frequency of the shifted infrared beam is locked to this reference Fabry-Perot cavity whose length is fixed. By changing the acousto-optic modulation frequency, which is provided by a computer-controlled frequency synthesizer, we can therefore precisely control the dye laser frequency over a range of 250 MHz centered at any desired frequency.

3. Study of the line profiles

After a two-photon excitation from the 2S metastable state, about 95% of atoms in the nD states undergo radiative cascade to the 1S ground state . The two-photon transition can then been detected by observing the corresponding decrease of the 2S beam intensity. Figure 3 shows a recording of the 2S intensity when the laser wavelength is swept through the $2S_{1/2}(F=1) - 10D_{5/2}$ transition of the hydrogen atom (the signal has been averaged over 10 scans). The signal amplitude corresponds to a 11% decrease of the metastable beam intensity. The experimental linewidth (in terms of total two-photon transition frequency) is 1.25 MHz, to be compared to the natural width of the transition which is 296 kHz.

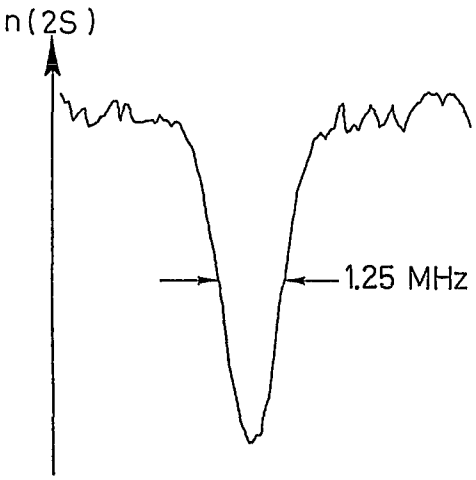

Figure 3 :
Recording of the $2S_{1/2}(F=1)-10D_{5/2}$ two-photon transition in hydrogen observed as a decrease of the metastable beam intensity n(2S).

There are several possible causes for the broadening and shift of the signal :

(i) The laser linewidth is responsible for a line broadening of 100 kHz.

(ii) Second order Doppler effect : for an atomic beam of 3.2 km/s mean velocity, the second-order Doppler effect decreases the line frequency by 44 kHz and broadens it by about 60 kHz.

(iii) Finite transit time /9/ : the geometry of an atomic beam gives a maximum line-broadening of 14 kHz corresponding to the largest possible angle of atomic trajectories with respect to the laser beams.

(iv) Light-shift and saturation : The laser beam waist inside the excitation chamber is $w_0 \simeq 600$ μm. For a 50W light power in each propagation direction, the light shift for an atom at rest in the center of the laser beam is about 560 kHz. Because the light power seen by each atom depends on its trajectory and varies along it, the light shift also contributes to the line broadening. For the same light power inside the excitation chamber 1m long, there is also a broadening effect due to the saturation of the two-photon transition (excitation rate 1.7×10^5 s^{-1}, transit time 2.8×10^{-4} s).

The line broadening due to light-shift and saturation is shown in Fig.4 where the experimental linewidth of the $2S_{1/2} - 10D_{5/2}$ transition in deuterium is reported versus the light intensity transmitted through the excitation cavity.

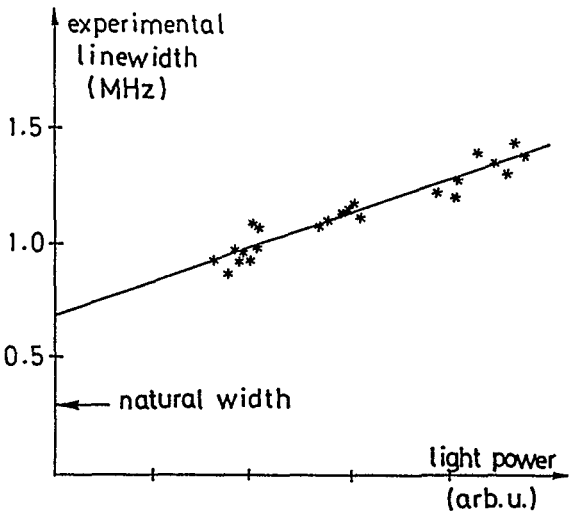

Figure 4 :
Example of the variation of the experimental linewidth as a function of the light power inside the excitation cavity. Data are relative to the $2S_{1/2} - 10D_{5/2}$ transition in deuterium ; the arrow indicates the natural linewidth of the transition

A numerical calculation of the line profiles due to the combined effect of the natural lifetime, the light-shift and the saturation has been performed taking into account all possible trajectories of atoms inside the metastable beam. Actually, the study of experimental linewidths shows there are some other stray effects responsible for the broadening of the lines. We have considered their contribution by making a convolution of the line profile with a gaussian curve.

As an example, Fig.5a shows the fit of an experimental signal relative to the transition $2S_{1/2} - 10D_{5/2}$ in hydrogen with the theoretical line profile obtained after this convolution. The parameters of the fit are the line

position, the light power and the gaussian broadening. The difference between the experimental and the fitted theoretical profiles is plotted in Fig. 5b which shows that there is no systematic error in the fit.

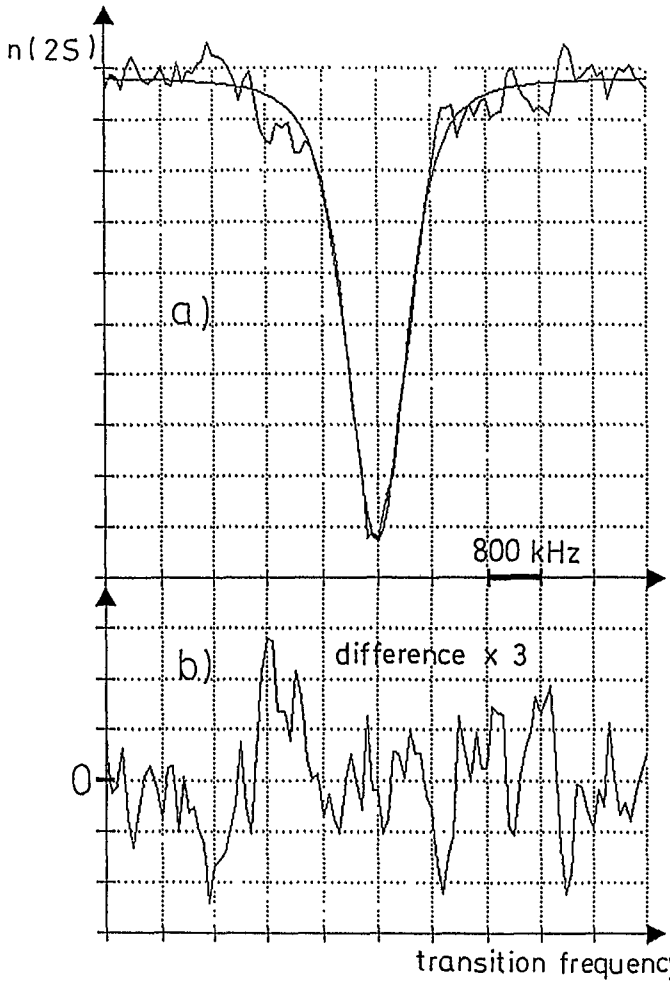

Figure 5 :
a) Fit of the experimental line profile ($2S_{1/2}$ - $10D_{5/2}$ in hydrogen) with the calculated one.
b) Difference in an expanded scale between the experimental and theoretical curves of a). For both graphs the frequency scale is in terms of the atomic transition frequency

The line position (relative to the frequency determined by the reference Fabry-Perot cavity) obtained from the fit is then investigated as a function of the light power (see Fig.6) ; extrapolation to zero light power gives the value corrected for light shifts.

Great care has been taken in the experimental set-up to avoid any stray field. In order to evaluate the effect of residual electric fields we have

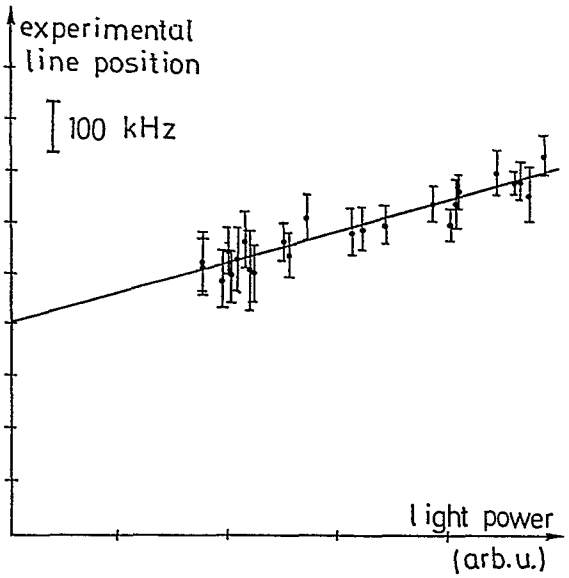

Figure 6 :
Example of an extrapolation of the two-photon line position versus the light power ($2S_{1/2}$-$10D_{5/2}$ transition in hydrogen)

excited the transitions to higher n because the Stark effect contribution to the line broadening varies as n^2. In Fig. 7 the signal for the 2S-20D transition is reported ; even on the assumption that the total broadening 950 kHz is due solely to the Stark effect and to the light shift, we obtain a stray field of 2mV/cm. As an example, the effect of such a low field on the $2S_{1/2}$- $10D_{5/2}$ transition is a broadening of $\sim$ 100kHz and a shift of $\sim$ 1kHz.

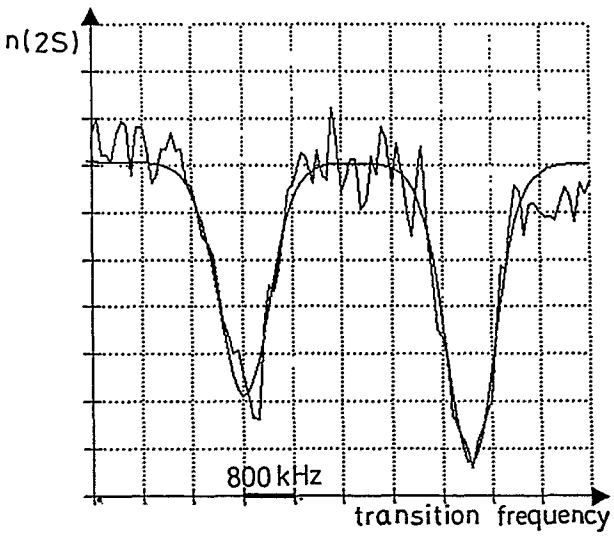

Figure 7 :
Same fit as that of Fig.5a) for the two fine structure components of the 2S-20D transition

4. Measurement of the transition wavelength

The absolute frequency position of the two-photon transition is measured by comparing the infrared dye laser wavelength with an I_2- stabilized He-Ne reference laser at 633 nm (see Fig.2). The key of the wavelength comparison is a nonconfocal etalon Fabry-Perot cavity (indicated as FPE in Fig.2) kept under a vacuum better than 10^{-6} mbar. This optical cavity is built with two silver-coated mirrors, one flat and the other spherical (R = 60 cm), in optical adhesion to a zerodur rod. Its finesse is $\sim$ 60 at 633 nm and $\sim$ 100 at 778 nm. An auxiliary He-Ne laser as well as the dye laser are mode-matched and locked to this Fabry-Perot cavity. Simultaneously the beat frequency between the auxiliary and etalon He-Ne lasers is measured by a frequency counter.

The frequencies at the red and infrared radiations inside the etalon Fabry-Perot cavity are determined by the resonant condition /10/

$$\upsilon = \frac{c}{2L} \left(N + \phi + \Phi \right)$$

where L is the cavity length, N is an integer number, ϕ is the reflective phase shift for light of frequency υ and Φ is the Fresnel phase shift

$$\Phi = \frac{1}{\pi} \cos^{-1} \left(1 - \frac{L}{R} \right)^{1/2}$$

The phase shift ϕ due to the mirror coatings is eliminated by the method of virtual mirrors /10/ by using two rods of different lengths (50cm and 10cm) for the Fabry-Perot. The Fresnel phase shift Φ is determined by measuring the frequency interval between the fundamental TEM_{00} mode and the first transverse mode TEM_{01} (or TEM_{10}). In principle TEM_{01} and TEM_{10} are degenerate by symmetry. However, due to imperfections in the mirror curvature, they are not exactly degenerate. Depending on the alignment of the laser beam with respect to the FPE optical axis, we may excite various superpositions of these two modes which give different results for the relative frequency of the first transverse mode and the TEM_{00} mode. We have made measurements for various alignments and the result is shown in Fig.8 which reports the dependence of this frequency difference upon the orientation of the transmitted light spots. The Fresnel phase-shift we need is then given by the mean value /11/ of the curve of Fig.8.

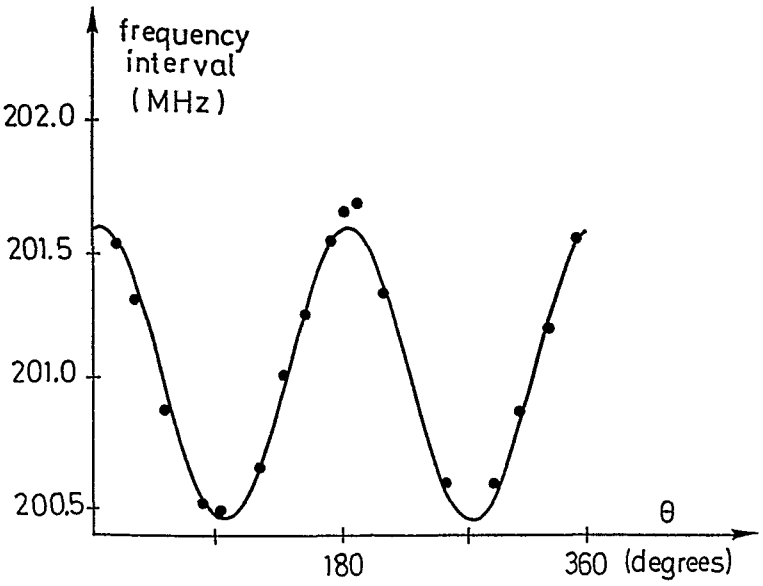

Figure 8 : Frequency interval between the fundamental mode and the first transverse mode of the Fabry-Perot etalon, measured as a function of the orientation of the plane of incidence of the auxiliary He-Ne laser. Similar behaviour has been observed for the dye laser radiation

Finally we have compared our reference I_2-stabilized He-Ne laser with that at the "Institut National de Métrologie" which had been previously compared with the standard He-Ne lasers of the "Bureau International des Poids et Mesures". As a result, the frequency of our reference laser relative to the lasers of the BIPM is known with a precision better than 10^{-11}.

5. Results

In both atomic hydrogen and deuterium we have studied the three transitions $2S_{1/2} - 8D_{5/2}$, $2S_{1/2} - 10D_{5/2}$ and $2S_{1/2} - 12D_{5/2}$. The frequencies measured, corrected for hyperfine splittings and for the second-order Doppler effect, are reported in Table I.

Table I

Transition	Frequency measured (MHz)	Rydberg constant -109737 (cm^{-1})
$2S_{1/2}$ - $8D_{5/2}$ in H	770649561.764 (38)	.3157130 (55)
$2S_{1/2}$ - $8D_{5/2}$ in D	770859253.058 (38)	.3157158 (55)
$2S_{1/2}$ - $10D_{5/2}$ in H	789144886.620 (39)	.3157136 (55)
$2S_{1/2}$ - $10D_{5/2}$ in D	789359610.444 (39)	.3157124 (55)
$2S_{1/2}$ - $12D_{5/2}$ in H	799191727.593 (40)	.3157120 (55)
$2S_{1/2}$ - $12D_{5/2}$ in D	799409185.185 (40)	.3157149 (55)

Using the theoretical work of Erickson /12/ for the 2P-nD interval and either the experimental value of the 2S Lamb-shift in hydrogen /13/ or the theoretical value of the 2S Lamb-shift in deuterium ($\mathcal{S}$ = 1059.229 MHz) /14/, we can deduce six independent determinations of the Rydberg constant. These values are in excellent agreement each with other. Our final result is :

$$R_\infty = 109\ 737.\ 315\ 7136\ (186)\ cm^{-1}.$$

The main source of error is due to the determination of the frequency of the standard laser /15/. In fact our precision with respect to this standard is less than 5×10^{-11}.

The various experimental errors are evaluated in Table II.

Table II : Estimated errors (parts in 10^{11})

Electron-to-proton mass ratio	1.1
Lambshift and energy level calculations	1.5
Stark effect	0.5
Statistical	1.4
Uncertainty of the theoretical line shape	2.0
Second-order Doppler effect	2.0
Ageing of the mirrors	1.8
Fresnel phase shift measurement	1.2
Comparison between the He-Ne lasers	1.0
Root mean square error	4.4
Standard laser	16.0
Final error	16.6

In Fig.9 our result is compared to those recently obtained by other groups, either from the Balmer transitions or from the 1S-2S transition assuming the theoretical value of the 1S Lamb-shift.

6. Conclusion

We have applied the Doppler-free two-photon technique to atomic hydrogen Rydberg states, and have achieved a new determination of the Rydberg constant. A more refined analysis of our results is at present in progress. As it stands, the main limitation of our determination is due to the frequency of the I_2 - stabilized He-Ne laser. This result shows that a new frequency standard is needed in the optical range. Moreover, since the hydrogen atom has transitions both in the visible and microwave ranges, the Rydberg constant may play a key role in the direct comparison between microwave and optical frequencies, as it has been pointed out in various occasions.

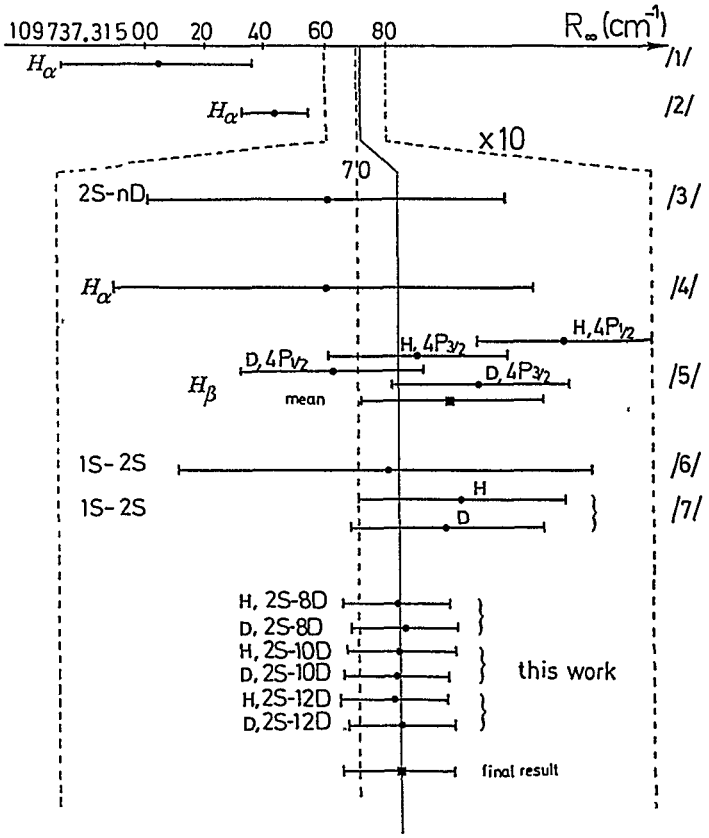

Figure 9 : Comparison of our result with those recently obtained by other groups

The authors are grateful to Prof. G.W. Series for critical reading of the manuscript. This research is supported in part by the "Bureau National de Métrologie".

REFERENCES

1. J.E.M. Goldsmith, E.W. Weber and T.W. Hänsch, Phys. Rev. Lett. 41, 1525 (1978)
2. S.R. Amin, C.D. Caldwell and W. Lichten, Phys. Rev. Lett. 47, 1234 (1981)
3. F. Biraben, J.C. Garreau and L. Julien, Europhys. Lett. 2, 925 (1986)
4. P. Zhao, W. Lichten, H.P. Layer and J.C. Bergquist, Phys. Rev. A34, 5138 (1986)
5 P. Zhao, W. Lichten, H.P. Layer and J.C. Bergquist, Phys. Rev. Lett. 58, 1293 (1987); and Proceedings of the VIIIth International Conference on Laser Spectroscopy (Are, June 1987): Laser Spectroscopy VIII edited by W. Persson and S. Svanberg (Springer Verlag, 1987) p.12
6. R.G. Beausoleil, D.H. McIntyre, C.J. Foot, E.A. Hildum, B. Couillaud and T.W. Hänsch, Phys. Rev. A35, 4878 (1987)
7. M.G. Boshier, P.E.G. Baird, C.J. Foot, E.A. Hinds, M.D. Plimmer, D.N. Stacey, J.B. Swan, D.A. Tate, D.M. Warrington and G.K. Woodgate, Nature 330, 463 (1987)
8. F. Biraben and L. Julien, Opt. Comm. 53, 319 (1985); and L. Julien, F. Biraben and B. Cagnac in Proceedings of Journée Thématique du B.N.M. (Paris, Sept. 1985): Bulletin du B.N.M. 66, 31 (1986)
9. F. Biraben, M. Bassini and B. Cagnac, J. Physique 40, 445 (1979)
10. H.P. Layer, R.D. Deslattes and W.G. Schweitzer, Appl. Opt. 15, 734 (1976)
11. C. Fabre, R.G. Devoe and R.G. Brewer, Opt. Lett. 11, 365 (1986)
12. G.W. Erickson, J. Phys. Chem. Ref. Data 6,, 831 (1977)
13. V.G. Pal'chickov, Yu.L. Sokolov and V.P. Yakovlev, Pis'ma Zh. Eksp. Teor. Fiz. 38, 347 (1983) (JETP Lett. 38, 418 (1983))
14. G.W. Erickson and H. Grotch, Phys. Rev. Lett. 60, 2611 (1988)
15. D.A. Jennings, C.R. Pollock, F.R. Petersen, R.E. Drullinger, K.M. Evenson, J.S. Wells, J.L. Hall and H.P. Layer,Optics Lett. 8, 136 (1983)